Bonding in Doped Gallium Nanoclusters: Insights from Regional DFT

David J. Henry,[a1] Kazuhide Ichikawa[b], Hiroo Nozaki,[b] Akitomo Tachibana,[b]

[a]*Chemical and Metallurgical Engineering and Chemistry, Murdoch University, Western Australia 6150, Australia*

[b]*Department of Micro Engineering, Kyoto University, Kyoto 606-8501, Japan*

Abstract: The molecular nature $(Ga_2)_n$ of gallium makes this an interesting metal to investigate for the development of novel nano-materials. However, establishment of a targeted approach to manipulating the properties of gallium clusters requires a detailed understanding of how doping affects the bonding in these species. In this study, the bonding of gallium nanoclusters has been investigated using electron deformation densities and Regional Density Functional Theory (RDFT). Bonding throughout $Ga_{12}X$ clusters is generally intermediate between covalent and metallic. However, the presence of Ga_2 subunits is clearly identified in clusters with endohedral dopants ($Ga_{12}X$, X = Al, Si, P, Ga, Ge, As). Although there is evidence of Ga_2 subunits in exohedral doped clusters, localized bonding to the dopant generally leads to significant disruption to the cluster framework. Maps of electronic chemical potential provide understanding for the observed differences in regioselectivity for hydrogen adsorption.

Keywords:

Gallium clusters, Regional DFT, covalent bonding, metallic bonding, Ga_2 sub-units, semi-metal

[1] Corresponding author: +(61 8) 9360 2681. E-mail: d.henry@murdoch.edu.au

1. Introduction

The high surface-to-bulk ratio of cluster-based materials provides new and unique surfaces for exploring chemical reactivity [1-4]. Although these materials have significant potential for catalysis and novel applications, the investigations of these materials for these purposes is often ad hoc rather than systematic. However, a detailed understanding of the bonding in clusters can be used to identify features that will facilitate manipulation of cluster properties for specific applications.

In bulk gallium metal, each atom has one very close neighbour at ~2.44 Å, while the other neighbours are found at 2.70 – 2.79 Å [5]. In this context, the shorter interactions might be considered as diatomic subunits (Ga_2) and bulk gallium might almost be considered a molecule material. Formation of Ga_2 subunits is also observed in the structure of many small clusters [6]. The molecular $(Ga_2)_n$ nature of bulk α-gallium has been proposed as an explanation for its low melting temperature (30 °C). Small particles of gallium are expected to have even lower melting temperatures due to the change in surface to volume ratio and the impact this has on cohesive energy [7]. In fact for particles composed of thousands of atoms the decrease in melting temperature is linked to particle radius [8]. However, experimental studies have revealed that many gallium clusters (< 500 atoms) exhibit melting temperatures substantially higher than the bulk [9-12]. Chacko et al. proposed that covalent bonding in small clusters explains the higher melting temperature of these species [13]. In contrast to this, separate studies by Núñez et al. [14] and Steenbergen and Gaston [15] suggest that these clusters have metallic or free-electron-like bonding. As Pyfer et al. note, the finite temperature behaviour of these clusters is directly linked to the geometry and bonding in the ground state [12]. Steenbergen and Gaston have explored this in some detail and have been able to link cluster structures to gallium bulk phases and the corresponding electronic states. This approach has provided insight to the size dependence of the electronic structure and the melting behaviour.

The electronic ground state of the Ga_2 molecule is $^3\Pi_u$ [16] with an experimental bond length of 2.75 Å [17]. The Ga_2 molecule formally has a bond order of 1, with the $2\sigma_g^+$ and one of the π_u orbitals singly occupied (Fig. 1). The single bond between the gallium atoms is formally covalent but clearly has both σ and π character. The long bond length of this electronic state arises largely from the σ overlap requirements of the $4p_x$ orbitals that form the $2\sigma_g^+$ molecular orbital. Tonner and Gaston also note that in the $^3\Sigma_g^-$ excited triplet state, the $2\sigma_g^+$ orbital is empty and now both of the π_u-orbitals are singly occupied. This leads to a formal bond order of one with only π-character but the electrons are more delocalized than in a typical π-bond [18].

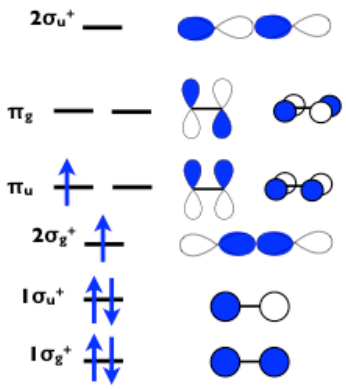

Figure 1. Qualitative molecular orbitals of Ga_2 in the $^3\Pi_u$ ground state.

Tonner and Gaston also recently investigated a number of small clusters and compared these with the structure of α-gallium [18]. Their density functional calculations clearly identify Ga_2 subunits as building blocks in Ga_4 and Ga_8 clusters. However, for Ga_6 the molecular orbitals appear to be built from a combination of Ga_2 and atomic orbitals, which highlights the complex nature of bonding in these species. Using Atoms in Molecules (AIM) analysis, they were able to show that the short interatomic distance in bulk α-gallium can be related to the $^3\Sigma_g^-$ state of Ga_2.

Although $(Ga_2)_n$ character of small clusters declines beyond Ga_8, it is noticeable that Ga_2 subunits are evident in the equatorial region of $Ga_{12}X$ clusters. However, as shown previously

[19] the Ga_2 subunits and axial bonds of these clusters are particularly sensitive to changes in the bonding environment within the cluster. In our recent study [20] we probed the reactivity of doped gallium nanoclusters and identified distinct regioselectivity for hydrogen adsorption. In particular, adsorption sites could be linked to the dopant and valence electronic configuration. In the pure Ga_{13} cluster, hydrogen adsorption occurs at or adjacent to the Ga_2 subunits. However, addition of dopants (Si, P, Ge or As) that increase the total number of valence electrons in the cluster leads to changes in the preferred adsorption sites. In particular, there is increased reactivity at the axial positions and decreased reactivity at hollow sites. Clusters with n-type dopants have a closed 1F shell within the Jellium model and in the case of $Ga_{12}P$ and $Ga_{12}As$, there is opening of the next electronic shell. This leads to more localized covalent bonding with hydrogen. In comparison, clusters with group 13 dopants have a partially filled 1F shell and generally exhibit delocalized bonding to hydrogen.

Previously [21,22] we have found that Regional Density Functional Theory (RDFT) analysis provides significant information regarding the bonding and reactivity of nanocluster species. The RDFT method revealed differences between the bonding inside aluminium cluster cages and those of the surface bonds that correlated with observed regioselectivity in reactions of the clusters. For example, metallic bonds generally hinder H_2 adsorption, whereas more covalent bonds favour H_2 adsorption.

The Regional DFT [23] and electronic stress tensor method were applied in this study to investigate the bonding in Ga_2 and $Ga_{12}X$ clusters (X = B, C, N, Al, Si, P, Ga, Ge or As) and to explain trends in hydrogen adsorption as a function of dopants.

2. Theoretical Procedures

The analysis carried out in this study was performed on the lowest energy endohedral (endo-$Ga_{12}X$) and exohedral (exo-XGa_{12}) isomers identified previously [19] at the PBE0/6-311G(d,p) level using the GAUSSIAN09 [24] computer program. Electronic stress tensor and energy density calculations were performed with the QEDynamics program package [25]

using the relevant electronic wavefunctions obtained from the PBE0/6-311G(d,p) structures. Electron deformation densities were obtained from PBE/DNP geometries using DMOL^3 [26,27]. All structures were confirmed as true minima using vibrational frequency analysis.

The RDFT and electronic stress tensor method have previously been reported in detail [28-31]. The zero kinetic energy isosurface was used to define the molecular surface of each cluster. The bond order indices (b_ε) reported in this study were obtained from the energy as:

$$b_\varepsilon = \frac{\varepsilon^S_{\tau\,AB}(\vec{r}_{Lagrange})}{\varepsilon^S_{\tau\,HH}(\vec{r}_{Lagrange})}, \qquad (1)$$

where $\varepsilon^S_{\tau\,AB}(\vec{r}_{Lagrange})$ and $\varepsilon^S_{\tau\,HH}(\vec{r}_{Lagrange})$ are the energy densities at the Lagrange points of the bond of interest (A-B) and the H—H bond of H_2 molecule, respectively. The regional electronic chemical potential μ_R is obtained from the ratio of energy density to electronic density [30,31]. Electron deformation density plots are shown for the 0.022 e/Å^3 iso-surface. VMD [32] and PyMol [33] were used for visualization of electronic stress tensor, bond indices and chemical potential.

3. Results and Discussion

A. Bonding in Ga_2. Previous studies have suggested that the structures of gallium clusters and the α-gallium bulk phase are strongly influenced by the tendency for gallium to form Ga_2 subunits [6,19]. It is therefore of interest to apply electron deformation density and RDFT analysis to investigate the bonding in Ga_2 before exploring the bonding in the $Ga_{12}X$ clusters. The electron deformation density identifies regions that have high electron density as a result of bonding interactions in the molecule or cluster. Figure 2 includes a plot of the electron deformation densities for the ground state ($^3\Pi_u$) and first triplet-excited-state ($^3\Sigma_g^-$) of Ga_2.

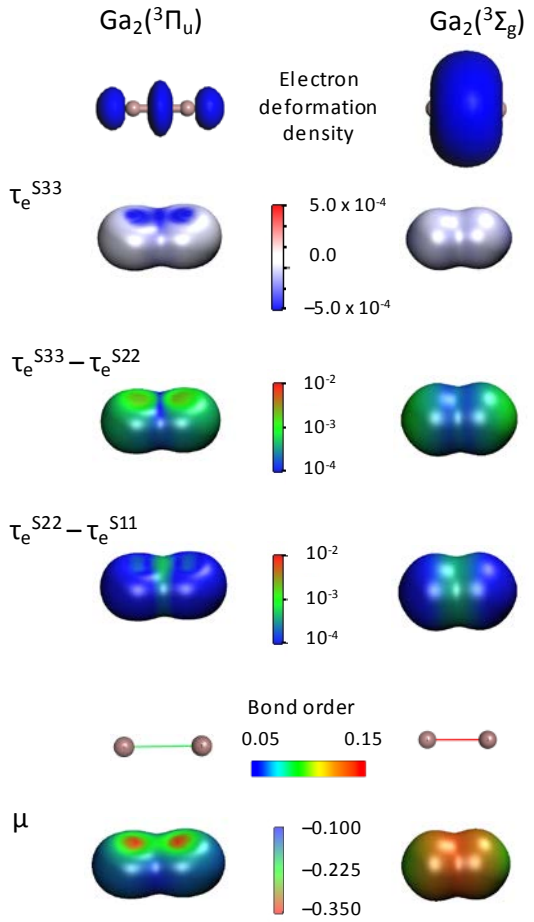

Figure 2. RDFT analysis of Ga_2 in the ground ($^3\Pi_u$) and first triplet excited ($^3\Sigma_g^-$) states.

The equilibrium bond length of the Ga_2 molecule arises from a balance between the competing atomic orbital interactions required to form the molecular orbitals. As noted in the Introduction, the long bond length of the $^3\Pi_u$ electronic state arises largely from the σ overlap requirements of the $4p_x$ orbitals that form the $2\sigma_g^+$ molecular orbital. However, the long interatomic distance weakens the bonding interaction between the $4p_y$ orbitals. Consequently, the $2\sigma_g^+$ molecular orbital is lower in energy than the π_u orbital and therefore makes a greater contribution to the bond energy in the $^3\Pi_u$ electronic state. The electron deformation density for the ground state of Ga_2 has the same spatial distribution as the $2\sigma_g^+$ molecular orbital, reflecting the contribution this orbital makes to bonding in the ground state. In comparison, the electron deformation density of the $^3\Sigma_g^-$ state is uniform and cylindrical, reflecting the equal contributions of the two singly occupied π_u orbitals to the bonding in this state.

The electronic stress method [28-31] provides information about the localization of electrons between pairs of atoms within a molecule. We denote the three eigenvalues of the electronic stress tensor in the ordering as follows: $\tau_e^{S33} > \tau_e^{S22} > \tau_e^{S11}$. If τ_e^{S33} is positive this corresponds to tensile stress and indicates localisation of electrons in these regions i.e. covalent character between a pair of atoms. However, if τ_e^{S33} is negative this corresponds to compressive stress, which generally indicates delocalization of the electrons in this region. This type of stress is observed in both metallic bonds and in short C≡C triple bonds of alkynes, due to the high concentration of electron density.

Figure 2 also displays maps of τ_e^{S33} on the electronic interface of the $^3\Pi_u$ and $^3\Sigma_g^-$ states of Ga_2. The variations in these maps correlate with the net bonding contributions arising from the valence 4p orbitals. It is clear that in the $^3\Pi_u$ state, τ_e^{S33} is very slightly negative across most of the surface of the molecule indicating that the electrons are not strongly localized. Furthermore there is a noticeable area of more negative τ_e^{S33} character, indicating compressive stress, in the bridge region along the x-y plane of the molecule. This arises from a weak bonding contribution from the singly occupied π_u molecular orbital due to poor overlap of the $4p_y$ valence orbitals at the interatomic distance of 2.71 Å. In comparison, the plot for the $^3\Sigma_g^-$ state exhibits a uniform τ_e^{S33} surface with no specific regions of high compressive stress. This is consistent with the stronger bonding in the π_u molecular orbitals due to greater overlap of the $4p_y$ and $4p_z$ valence orbitals at the shorter interatomic separation of this electronic state (2.45 Å).

The differential eigenvalues $\tau_e^{S33} - \tau_e^{S22}$ and $\tau_e^{S22} - \tau_e^{S11}$ can be used to quantify degeneracy amongst the three eigenvalues of the stress tensor, which can highlight important features of the different types of bonding. Covalent bonds exhibit strong directionality with one positive eigenvalue substantially larger than the other two. Covalent bonding in hydrocarbons is reflected by $\tau_e^{S33} - \tau_e^{S22}$ values in the range 0.1 – 1 and $\tau_e^{S22} - \tau_e^{S11}$ values in the range 0 – 0.04. In comparison, the strong metallicity of the alkali metal species is demonstrated by the very small values obtained for both $\tau_e^{S33} - \tau_e^{S22}$ and $\tau_e^{S22} - \tau_e^{S11}$. Figure

2 displays maps of the differential eigenvalue $\tau_e^{S33} - \tau_e^{S22}$ on the electronic surface of the two lowest energy triplet electronic states of Ga_2. The $\tau_e^{S33} - \tau_e^{S22}$ differential eigenvalues for the $^3\Pi_u$ state vary across the molecule with the smallest values at the centre of the bond and a gradual increase in the values moving away from the bonding region. This indicates that τ_e^{S33} and τ_e^{S22} are almost degenerate in the centre of the molecule but differ at the axial extremes of the molecule. In comparison, $\tau_e^{S22} - \tau_e^{S11}$ values are largest at the centre of the bond and decrease moving away from the bond, indicating that the τ_e^{S22} and τ_e^{S11} are degenerate across most of the molecular surface. Again, this pattern is consistent with net bonding contributions arising from the singly occupied $2\sigma_g^+$ and π_u orbitals of the ground state. In particular, the $2\sigma_g^+$ orbital is bonding along the molecular axis with large lobes also located outside the bond, which corresponds with the largest $\tau_e^{S33} - \tau_e^{S22}$ values. In comparison, the π_u orbital does not lead to strong localization of the electron in the interatomic region and this contributes to the small $\tau_e^{S33} - \tau_e^{S22}$.

The $\tau_e^{S33} - \tau_e^{S22}$ values for the $^3\Sigma_g^-$ state exhibit a similar distribution to that of the $^3\Pi_u$ state but the small values extend further from the centre of the bond and the values in the axial atop regions are larger than for $^3\Pi_u$ state. This is consistent with a bond consisting primarily of π-character. The $\tau_e^{S22} - \tau_e^{S11}$ differential values indicate that τ_e^{S22} and τ_e^{S11} are degenerate across most of the molecular surface.

As noted in the Introduction, the long bond length of the ground state of Ga_2 largely arises from a need to balance the nuclear repulsion energy with the competing σ and π overlap requirements of the $4p_x$ and $4p_y$ orbitals. In the $^3\Sigma_g^-$ excited state, net bonding arises from the two degenerate π_u orbitals, which are formed from equivalent overlap of the $4p_y$ and $4p_z$ orbitals, leading to a shorter bond length. Consequently, the energy density bond order is slightly higher for the $^3\Sigma_g^-$ state than for the $^3\Pi_u$ state. Nevertheless, both values are substantially smaller than the unity value found for the fully covalent σ-bond of H_2. The behavior in both of these electronic states of Ga_2, indicates bonding character that is intermediate between covalent and metallic, consistent with other semi-metal systems

[34,35]. Inspection of the chemical potential plots indicates that the most electrophilic region of the $^3\Pi_u$ state is the bridge region, which facilitates the addition of hydrogen across the Ga-Ga bond as in Ga_2H_6. The $^3\Sigma_g^-$ state is electrophilic near the centre of the bond with values decreasing slightly moving away from the bond.

B. Structure and Bonding of endo-$Ga_{12}X$. As reported previously, [19,36-38] the pure Ga_{13} cluster has a distorted decahedral structure. Consequently, the two 5-membered rings in the equatorial region of the cluster are in an eclipsed arrangement so that each of these Ga atoms has a nearest neighbor in the opposing ring at ~ 2.6 Å. These pairs of atoms can be considered as Ga_2 subunits. Our earlier study [19] explored an extensive range of endohedral doped isomers including icosahedral and decahedral structures. For clusters doped with third- and fourth-row p-block elements the structures with decahedral-like symmetry were identified as the lowest in energy. The $Ga_{12}Si$ and $Ga_{12}Ge$ clusters have 40 valence electron configurations, which corresponds with a stable closed shell electronic configuration within the Jellium model and therefore they exhibit the most compact structures. In comparison, when doping the core of the clusters with second-row p-block dopants the isomers with icosahedral-like symmetry are lowest in energy, with the 40-electron cluster (endo-$Ga_{12}C$) again being the most compact of the three clusters.

The deformation densities for the icosahedral gallium clusters with X = B, C or N, generally have the same features as the isoelectronic $Al_{12}X$ clusters (Fig. 3a). In particular, the electronic charge forms a framework throughout the cluster with the highest densities located in the interstitial regions. This corresponds with development of metallic or Jellium-like bonding and compares well with earlier studies of Al_{13}, Al_{13}^- and $Al_{12}Si$ [39-43]. As reported previously this is also evidenced by the high degree of degeneracy in the eigenvalue spectrum of endo-$Ga_{12}C$ [19,44]. In addition to the delocalised framework, there is significant charge concentrated about the core atom of these endo-$Ga_{12}X$ clusters. Sun et al. [42] noted similar behaviour for $Al_{12}Si$, with the excess charge from the core silicon atom distributed in

bonds between the core and the cage Al atoms. As the electronegativity of the core atom increases these regions of electron density become more contracted.

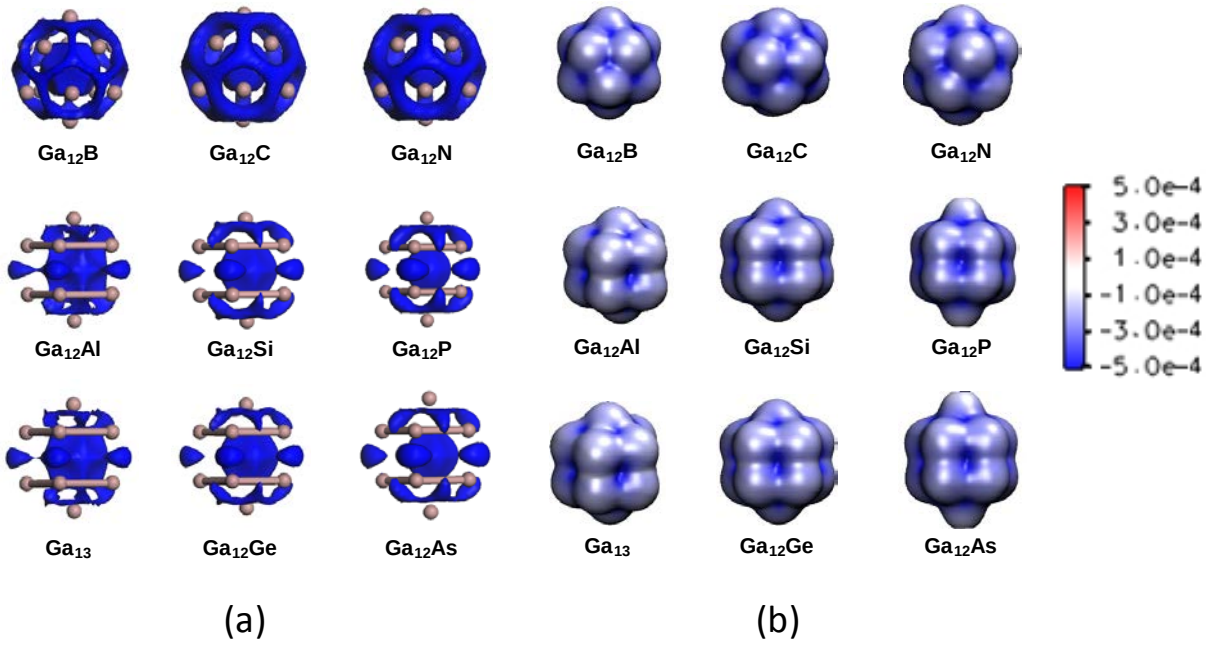

Figure 3. (a) Electron deformation densities for endohedral $Ga_{12}X$ clusters and (b) Maps of τ_e^{S33} on the electronic interfaces of endohedral gallium clusters.

The deformation density isosurfaces of endo-$Ga_{12}X$ clusters with third- and fourth-row dopants are quite different, with delocalised metallic framework only observed between the axial and equatorial atoms. In comparison, there is a small region of very localised charge density in the centre of each of the Ga_2 subunits of the equatorial region. This localised density is very similar to the bonding in the ground state of Ga_2 and is evidence of residual covalent character between these atoms. These clusters also exhibit a concentration of charge about the core dopants, which becomes more contracted with electronegativity of the dopant atom. Consequently, this region of density is least contacted in the endo-$Ga_{12}Al$ and Ga_{13} clusters and in fact merges with the delocalised density of the axial regions and to a lesser with the density of the Ga_2 sub units. We have shown previously [19] that endo-$Ga_{12}X$ clusters with X = Al, Si, Ga and Ge, are less Jellium-like than their icosahedral counterparts

and this is consistent with the less developed electron deformation density framework observed in these species.

Figure 3b displays maps of τ_e^{S33} on the electronic interface of endohedral gallium clusters. As can been seen from these maps, τ_e^{S33} has a slightly negative value across most of the surface, indicating slight compressive stress throughout the clusters. The most negative (blue) regions are located in the centre of the hollow faces of the clusters indicating significant delocalisation of the electron density in these regions, which generally correlates well with the regions of highest electron density in the electron deformation density plots (Fig. 3a). However, in the bridge locations between pairs of atoms, the τ_e^{S33} values are only slightly negative suggesting that the electrons are not fully delocalised and bonding is intermediate between covalent and metallic. Figure 3b also suggest that the Ga_2 subunits of the decahedral clusters show the least metallic character, particularly for the 39 valence electron clusters ($Ga_{12}Al$ and Ga_{13}). In fact the τ_e^{S33} surfaces for each of these pairs of atoms bear a close resemblance to the τ_e^{S33} surface of the $^3\Pi_u$ state of Ga_2. In comparison, τ_e^{S33} values between atom pairs of the icosahedral clusters are quite uniform across the surfaces of the clusters. However, the variations in τ_e^{S33} surfaces suggest an increase in metallic character from $Ga_{12}B$ through to $Ga_{12}N$.

Covalent bonds are identified within the RDFT scheme by a positive largest eigenvalue and strong directionality. The recent study on lithium clusters has shown that metallic bonding is characterized by negative values for the three eigenvalues of the electronic stress tensor, with no particular directionality [22]. Metalloid bonds generally exhibit slightly negative eigenvalues with some directionality. Figure 4 displays a plot of τ_e^{S33} at the Lagrange points of Ga cluster bonds versus bond length. As noted above the τ_e^{S33} values are generally slightly negative and therefore intermediate between fully covalent and metallic i.e. they are metalloid. However, the magnitude of the τ_e^{S33} values decreases with bond length. In fact there is almost a linear correlation between τ_e^{S33} and bond length for the surface Ga-Ga bonds of the endo-$Ga_{12}X$ clusters. Therefore, the longest bonds exhibit the least

delocalization of the local electron density, which would correspond with less π-character between these atoms. The Ga-X bonds for the endohedral doped clusters with decahedral symmetry (X = Al, Si, P, Ga, Ge or As) exhibit similar behaviour to Ga-Ga bonds. In comparison, the Ga-X bonds of endo-$Ga_{12}B$, endo-$Ga_{12}C$ and endo-$Ga_{12}N$ are found to have τ_e^{S33} values very close to zero and therefore exhibit less delocalization of the electron density than a Ga-Ga bond of the same length. This corresponds with the concentration of charge about the core dopants of these icosahedral-like clusters.

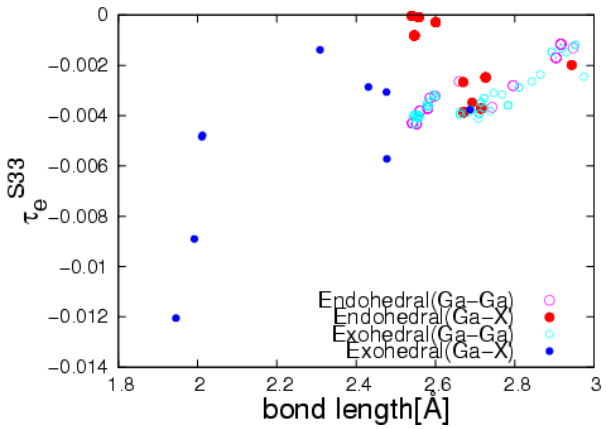

Figure 4. Plot of τ_e^{S33} versus bond length for gallium clusters ($Ga_{12}X$).

The $\tau_e^{S33} - \tau_e^{S22}$ values (Figure SF1a, Supp Info) are generally quite small across the surfaces of the clusters. However, $\tau_e^{S33} - \tau_e^{S22}$ values in atop positions are an order of magnitude higher than those of the hollow positions. The eigenvalue maps also indicate that the Ga_2 subunits of the equatorial region exhibit the least degeneracy between τ_e^{S33} and τ_e^{S22} which is indicative of more covalent character in these regions. Maps of the $\tau_e^{S22} - \tau_e^{S11}$ differential eigenvalue (Figure SF1b, Supp Info) also highlight the difference in bonding between atoms of the Ga_2 subunits and other atomic pairs in these clusters.

Figure 5a provides a plot of $\tau_e^{S33} - \tau_e^{S22}$ vs $\tau_e^{S22} - \tau_e^{S11}$ values for a range of different species including covalently bonded hydrocarbons, alkali metal clusters, aluminium clusters and our doped gallium clusters.

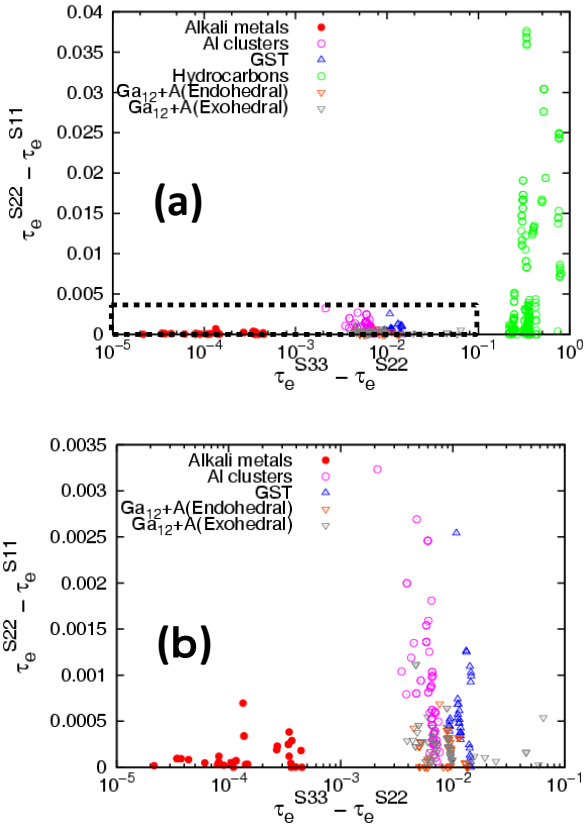

Figure 5. (a) Plots of $\tau_e^{S33} - \tau_e^{S22}$ vs $\tau_e^{S22} - \tau_e^{S11}$ for a range of different species and bond types and (b) an enlargement of the metal and semimetal region.

Covalent bonding in hydrocarbons is reflected by $\tau_e^{S33} - \tau_e^{S22}$ values in the range 0.1 – 1 and $\tau_e^{S22} - \tau_e^{S11}$ values in the range 0 – 0.04. In comparison, the strong metallicity of the alkali metal species is demonstrated by the very small values obtained for both $\tau_e^{S33} - \tau_e^{S22}$ and $\tau_e^{S22} - \tau_e^{S11}$. Tachibana and co-workers [34,35] have shown previously that in semimetal species such as Al_n clusters and $Ge_2Sb_2Te_5$ (GST), the bonding is intermediate between covalent and metallic. The differential eigenvalues for our gallium clusters also clearly fall in this semimetal range. Figure 5b displays an enlargement of the region of the alkali and semimetal species. Although the $Ga_{12}X$ cluster values are in the same region as the values for Al clusters and GST, there are subtle differences between the systems. For example, aluminium clusters exhibit only a small range of $\tau_e^{S33} - \tau_e^{S22}$ values but a large range for $\tau_e^{S22} - \tau_e^{S11}$. In comparison, our $Ga_{12}X$ clusters exhibit a large spread of $\tau_e^{S33} - \tau_e^{S22}$ values

but a small spread of $\tau_e^{S22} - \tau_e^{S11}$ values. This again reflects the differences in bonding between the Ga_2 subunits and the other atomic pairs within the clusters.

Energy density bond indices (b_ε) were calculated where Lagrange points could be located between adjacent atoms and are shown as coloured lines in Figure 6.

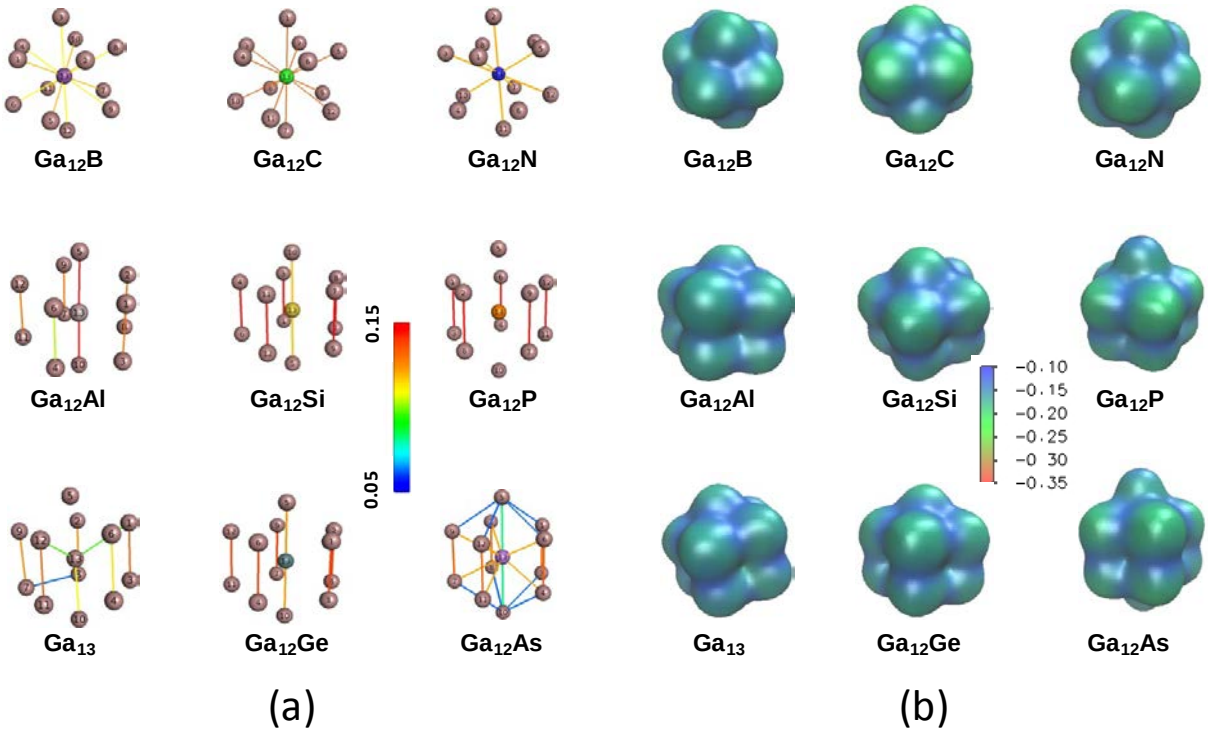

Figure 6. (a) Energy density bond indices (b_ε) and (b) maps of electronic chemical potential for endohedral doped ($Ga_{12}X$) clusters.

Significant differences can be seen between the group of clusters with second-row dopants and those with third- and fourth-row dopants. Firstly, for the endo-$Ga_{12}B$, endo-$Ga_{12}C$ and endo-$Ga_{12}N$ clusters, Lagrange points were only identified inside the clusters, between the core dopant and the surface gallium atoms. This is the same region as the concentrated charge identified in the deformation densities and coincides with the Jellium 1P and 2P shells that are composed of bonding orbitals between the core and the surface. It is clear from the b_ε bond-order plots that the largest bond order indices are found in the highly stable 40 valence electron cluster, endo-$Ga_{12}C$, followed by the endo-$Ga_{12}N$ and then the endo-$Ga_{12}B$ clusters.

The 1P and 2P shells are well developed in these clusters and the bond indices correlate with the increasing degeneracy in each of these sets of orbitals. Nevertheless, we find bond indices of only ~ 10% of the value of the H-H bond and this reflects only a low level of covalency between core and surface atoms.

The endo-$Ga_{12}X$ clusters with third and fourth row dopants have lower symmetry than the icosahedral-like clusters described above and exhibit quite different patterns of bond indices. In particular, relatively few Lagrange points were located inside the clusters, which coincides with breaking of the degeneracy in the 1P and 2P Jellium shells. In contrast, many Lagrange points were located between pairs of surface atoms, particularly for the Ga_2 subunits of these clusters. The bond indices for the equatorial Ga_2 subunits of $Ga_{12}Al$, $Ga_{12}Si$ and $Ga_{12}P$ follow the pattern of bond lengths. For example, in $Ga_{12}Al$ one of the Ga_2 subunits is elongated relative to the other four and this pair of atoms have a significantly weaker bond. In comparison the equatorial Ga_2 bonds of the $Ga_{12}Si$ and $Ga_{12}P$ clusters are consistently stronger. There is a systematic decrease in the bond indices between the dopant X and the axial gallium atoms across this series of clusters. These patterns of bond indices are consistent with the observed regioselectivity for hydrogen adsorption on the cluster surfaces [20]. For example, in $Ga_{12}Al$ the highest reactivity is generally observed in the region of the Ga_2 subunits, which have weaker bonding than the axial Ga-X bonds. The $Ga_{12}Si$ and $Ga_{12}P$ have increased reactivity in the axial regions due to a weakening of the axial Ga-X bonds, while decreases in reactivity at the equatorial Ga_2 sub units correspond with increases in bond index. Both the bond indices and the regioselectivity can be understood in terms of the occupations of the frontier orbitals of these clusters. Due to a Jahn-Teller distortion, the HOMO of the 39 valence electron clusters is a singly occupied bonding orbital located in the equatorial region. The lobes of this orbital correspond with the Ga_2 subunits. In the 40 valence electron clusters, the HOMO is doubly occupied and part of the degenerate set of Jellium orbitals, which increases the bonding character and the bond indices in the Ga_2 subunits. In the 41 valence electron systems, there is opening of the next Jellium shell. This again leads to a Jahn-Teller distortion, in this case along the axis of the cluster, which results

in a weakening of the bonding in the Ga_2 subunits. However, again we find that the average b_ε values in our endo-$Ga_{12}X$ clusters are ~5 – 15 % of the value for the H-H bond indicating only a low level of covalency.

The overall features of the bonding in the fourth-row doped clusters are generally similar to the third-row doped species but the b_ε are generally smaller. This can be linked to the larger size of the core atoms in these clusters that induces strain in the Ga_{12} cage. For example, the Jahn-Teller distortion in Ga_{13} is larger than in $Ga_{12}Al$, leading to a broader distribution of b_ε values for the Ga_2 subunits. Furthermore, the core Ga is not located equidistant from both axial atoms therefore these bonds have different bond indices. The bonding patterns for $Ga_{12}Ge$ and $Ga_{12}As$ closely reflect those of $Ga_{12}Si$ and $Ga_{12}P$, respectively, but as noted above, the absolute b_ε values are slightly smaller.

The chemical potential (μ) maps identify variations in electrophilicity across the surface of the clusters (Fig. 6b). Regions with higher electrophilicity are identified with more negative μ values, whereas regions with weaker μ (less negative) are generally more nucleophilic. It is clear from Figure 6b that the atop positions of all of the endo-$Ga_{12}X$ clusters exhibit the most negative μ values and therefore are the most electrophilic regions of the clusters. Comparison across a series reveals that the surface atoms are increasingly deshielded with increasing electronegativity of the core atoms, reflecting the transfer of charge density towards the core. In comparison, the bridge and hollow positions of the clusters have less negative μ values and can be considered more nucleophilic. In general, hydrogen atom is adsorbed in electrophilic regions of the clusters. As the electronegativity of the core dopant increases, so does the electrophilicity of the surface and the bonding to H atom becomes increasingly more localised. Consequently, adsorption in equatorial fourfold hollow sites is only observed in the Ga_{13} and endo-$Ga_{12}Al$ clusters. In comparison, the endo-$Ga_{12}P$ and endo-$Ga_{12}As$ clusters exhibit a clear preference for localized bonding to H atom in the axial and equatorial atop positions. The endo-$Ga_{12}Si$ and endo-$Ga_{12}Ge$ clusters are intermediate between these two extremes.

C. Structure and Bonding of exo-$Ga_{12}X$

In this section we discuss the trends in the bonding of exohedrally doped gallium clusters (exo-XGa_{12}). The exo-$Ga_{12}X$ isomers have similar cage structures to their endohedral counterparts. Nevertheless, locating the dopant in the cluster surface leads to a loss of symmetry and generally destabilises the clusters relative to the corresponding endo-$Ga_{12}X$ isomers [19]. In the case of X = Al, the destabilisation is marginal (+0.02 eV), whereas for X = P and Si, the effect is quite large (+0.40 and +0.61 eV). Lighter element exohedral dopants introduce significant structural distortion but the energetic effect is element specific. For example, the exo-CGa_{12} isomer is significantly higher in energy (+0.70 eV) than endo-$Ga_{12}C$, whereas exo-NGa_{12} is slightly lower in energy (-0.10 eV) than endo-$Ga_{12}N$.

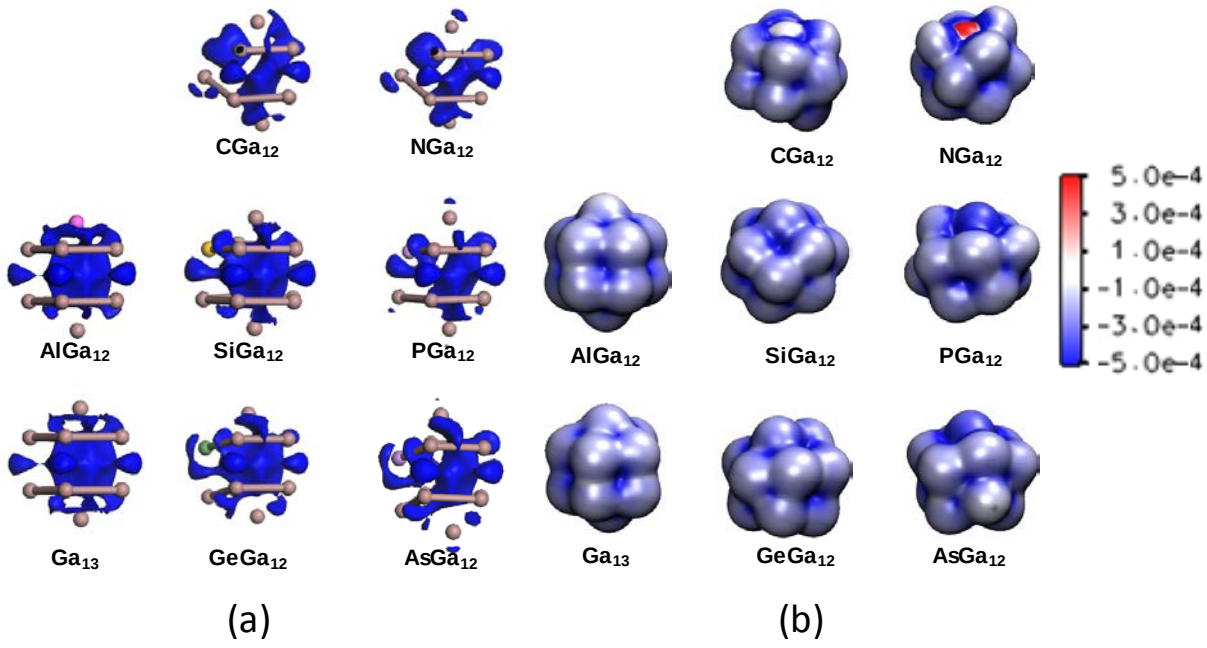

Figure 7. (a) Electron deformation densities (0.02 electrons $Å^{-3}$) for exohedral $Ga_{12}X$ clusters and (b) Maps of τ_e^{S33} on the electronic interfaces of exohedral gallium clusters.

Comparison of Figures 3a and 7a reveals that the deformation density of exo-$AlGa_{12}$ is quite similar to that of endo-$Ga_{12}Al$ and the undoped Ga_{13}, with delocalised bonding throughout the core and the axial region and localised bonding at the centre of the Ga_2 subunits. This indicates that the axial aluminium dopant exerts only a small perturbation on

the bonding of the system. The deformation densities of the equatorial doped exo-$SiGa_{12}$ and exo-$GeGa_{12}$ clusters differ significantly from their endohedral counterparts but bear similar features to exo-$AlGa_{12}$. These include delocalised charge throughout the core region that extends to the axial region and charge density at the centre of the Ga_2 subunits. However, there is concentration of charge around the dopant site of each of these cluster reflecting their greater electronegativity. The redistribution of charge density towards the dopant is further enhanced in the exo-PGa_{12} and exo-$AsGa_{12}$ clusters so that there is a significant reduction in charge density in the axial regions which corresponds with the weakening and lengthening of the X-Ga_{ax} bonds. Charge density is also concentrated around the dopant atoms in exo-CGa_{12} and exo-NGa_{12} and this substantially disrupts the bonding, leading to significant distortion of the cluster symmetry.

Figure 7b displays maps of τ_e^{S33} on the electronic interface of exohedral gallium clusters. As for the endohedral-doped clusters, τ_e^{S33} generally has a slightly negative value across most of the surface, indicating compressive stress throughout the clusters. For most of this group of clusters, the most negative (blue) regions are located in the centre of the hollow faces of the clusters indicating significant delocalisation of the electron density in these regions. The τ_e^{S33} values are generally only slightly negative in the bridge locations, suggesting that the electrons are not fully delocalised and bonding is intermediate between covalent and metallic. However, for some clusters the presence of the dopant at the surface does lead to some significant local effects. For example, τ_e^{S33} is close to zero around the aluminium atom of exo-$AlGa_{12}$ and the carbon atom of exo-CGa_{12} indicating less delocalisation of electrons in this region relative to the other regions of the cluster surface. We also find that τ_e^{S33} is positive around the nitrogen atom of exo-NGa_{12} indicating localised covalent bonding. In comparison, τ_e^{S33} is negative around the P and As atoms of exo-PGa_{12} and exo-$AsGa_{12}$, respectively, indicating increased delocalisation of electrons in these regions.

As for the endohedral clusters, the magnitude of the τ_e^{S33} values for Ga-Ga bonds of the exohedral clusters decrease almost linearly with increasing bond length (Fig. 4). In

comparison, the τ_e^{S33} values for Ga-X bonds of these clusters exhibit a less systematic variation. The values that show the largest deviation from the linear trend are the short Ga-C bonds of the exo-CGa_{12} cluster and to a lesser extent the Ga-N bonds of exo-NGa_{12}. The more negative τ_e^{S33} values of these clusters imply metallic bonding in these regions. However, this may also be due to the high concentration of electron density in these regions.

The $\tau_e^{S33} - \tau_e^{S22}$ values (Figure SF2, Supp Info) are generally quite small across the surfaces of the clusters and indicate that electrons are delocalised in the hollow regions of each cluster and around the Al atom of exo-$AlGa_{12}$. In comparison, there is an increase of electron localisation around the carbon and nitrogen atoms of exo-CGa_{12} and exo-NGa_{12}. The $\tau_e^{S22} - \tau_e^{S11}$ differential eigenvalues are very small across most of the surface of the clusters, with the largest values identified between Ga atoms of the Ga_2 subunits and between the dopants and neighbouring gallium atoms of exo-CGa_{12} and exo-NGa_{12}. Figure 5 includes a plot of $\tau_e^{S33} - \tau_e^{S22}$ vs $\tau_e^{S22} - \tau_e^{S11}$ values for exohedral-doped clusters. The values for the exohderal clusters fall in the same region as the endohedral clusters, again implying that overall the bonding in these species is intermediate between covalent and metallic.

The exo-XGa_{12} clusters with third and fourth row dopants have similar distributions of bond indices to their endohedral counterparts (Fig. 8a). In particular, equatorial Ga-Ga bonds generally have larger b_ε values than the axial Ga-X bonds. The systems with second-row dopants exhibit significant distortion away from the icosahedral symmetry, which can be understood by the preference to form strong short bonds between the dopant and the neighbouring gallium atoms. This leads to a weakening of many of the other bonds throughout the cluster relative to corresponding endo-$Ga_{12}X$ clusters.

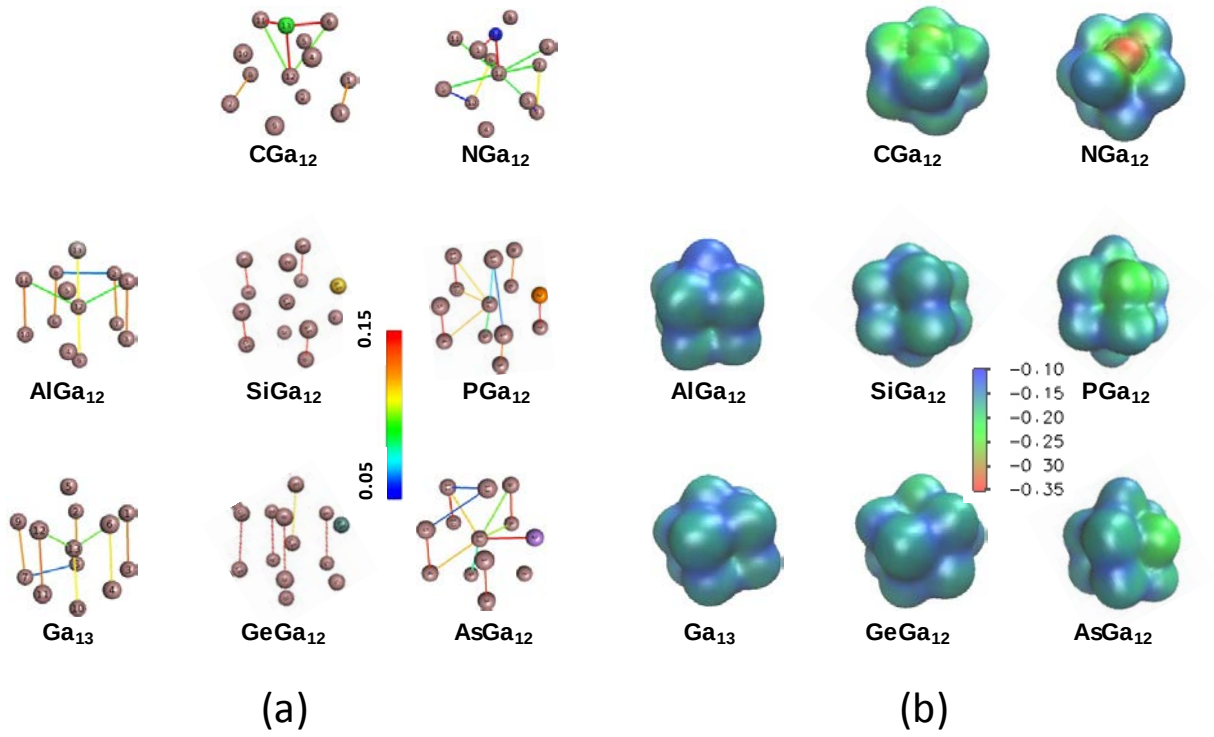

Figure 8. (a) Energy density bond indices (b_ε) and (b) maps of electronic chemical potential for exohedral doped (XGa_{12}) clusters.

The chemical potential maps for the decahedral-like exo-XGa_{12} clusters indicate that the surface gallium atoms are generally deshielded, making these regions electrophilic (Fig. 8b). Bridge positions tend to be less electrophilic than the atop positions. The largest differences in chemical potential are observed around the dopant atoms. For the exo-XGa_{12} clusters, μ becomes successively more negative around the dopant for the series X = Al, Si and P, with the Al atom being less electrophilic and P being substantially more electrophilic than the surface gallium atoms of the respective clusters. A similar trends is observed for the X = Ga, Ge, As series of clusters but the μ values around the X atoms are generally slightly smaller in magnitude. The region around the dopant atoms of exo-CGa_{12} and exo-NGa_{12} are also highly electrophilic.

4. Conclusions

Electron deformation density plots and Regional Density Functional Theory (RDFT) have been used in this study to investigate the bonding of Ga_2 and $Ga_{12}X$ clusters. Clear differences are identified in the bonding characteristics of the ground ($^3\Pi_u$) and first excited triplet ($^3\Sigma_g^-$) states of Ga_2 that can be used to identify the presence of Ga_2 subunits in larger clusters.

The electronic properties of the icosahedral based endo-$Ga_{12}X$ clusters with second-row p-block dopants are generally very similar to isoelectronic $Al_{12}X$ clusters. The small size of the core dopant in these systems combined with their electronegativity relative to gallium results in charge being transferred from the surface atoms towards the core. The concentration of charge between the core and the surface atoms provides evidence for the establishment of a metallic or Jellium-like bonding in these species.

The larger size and smaller electronegativity of 3rd and 4th row dopants, relative to gallium, leads to quite a different charge distribution in the endo-$Ga_{12}X$ clusters with X = Al, Si, P, Ge or As. Although there is electron delocalisation around the core and axial regions of these clusters, there is also strong evidence of Ga_2 subunits in the equatorial region.

RDFT analysis of the endo-$Ga_{12}X$ clusters reveals bond properties intermediate between metallic and covalent, consistent with semimetal materials. The RDFT analysis also reveals similarities between the bonding in the Ga atoms of the equatorial region of the endo-$Ga_{12}X$ clusters and the ground state of the Ga_2 molecule. The calculated b_ε bond indices and surface maps of electronic chemical potential provide understanding for the previously observed regioselectivity for hydrogen atom adsorption [20]. The significant deshielding around the surface atoms, caused by migration of charge towards the core, suggests that these clusters will interact strongly with nucleophiles and Lewis bases. These results clearly explain the previously reported variations in regioselectivity for H atom adsorption across this series of clusters.

Exohedral doping with second-row p-block dopants leads to a large concentration of charge density around the dopants that significantly distorts the cluster geometry. The third- and fourth-row elements (X = Al, Si, P, Ge and As) generally cause only a minor perturbation to the geometry of the cluster when used as exohedral dopants. This can again be attributed to their similar size and electronegativity to gallium. RDFT analysis reveals that the surface atoms of the exo-XGa_{12} clusters are also generally deshielded and therefore electrophilic. This is most evident in the region of the dopants.

Acknowledgements. We gratefully acknowledge allocation of computing time from the Australian National Computational Infrastructure (NCI) facility.

Supporting Information. Figures containing maps of $\tau_e^{S33} - \tau_e^{S22}$ and $\tau_e^{S22} - \tau_e^{S11}$ differential eigenvalues, on the electronic interfaces of all gallium clusters considered in the present work.

References

[1] Metal Clusters; Moskovits, M., Ed.; Willey and Sons, 1986.

[2] Clusters of Atoms and Molecules: Theory, Experiment and Clusters of Atoms; Haberland, H., Ed.; Springer Series in Chemical Physics, v. 52, Springer Verlag, 1995.

[3] Clusters and Nanomaterials, Kawazoe, Y., Ohno, K., Kondow, T., Eds.; Springer, 2002.

[4] Clusters and Nano-Assemblies, Jena, P., Khanna, S. N., Rao, B. K., Eds.; World Scientific: Singapore, 2005.

[5] Greenwood, N. N.; Earnshaw, A. Chemistry of the Elements; Pergamon Press: Oxford, U.K., 1984.

[6] N. Gaston, A.J. Parker, Phys. Lett. 501 (2011) 375-378.

[7] P. Pawlow, Z. Phys. Chem., Stoechim. Verwandtschaftsl. 65 (1909) 545.

[8] P.R. Couchman, W.A. Jesser, Nature 269 (1977) 481-483.

[9] G.A. Breaux, R.C. Benirschke, T. Sugai, B.S. Kinnear, M.F. Jarrold, Phys. Rev. Lett. 91 (2003) 215508

[10] G.A. Breaux, D.A. Hillman, C.M. Neal, R.C. Benirschke, M.F. Jarrold, J. Am. Chem. Soc. 126 (2004) 8628-8629.

[11] G. A. Breaux, B. Cao, M.F. Jarrold, J. Phys. Chem. B. 109 (2005) 16575-16578.

[12] K. Pyfer, J.O. Kafader, A. Yalamanchali, M.F. Jarrold, J. Phys. Chem. A 118 (2014) 4900-4906.

[13] S. Chacko, K. Joshi, D.G. Kanhere, Phys. Rev. Lett. 92 (2004) 135506.

[14] S. Núñez, J.M. López, A. Aguado, Nanoscale 4 (2012) 6481-6492.

[15] K. G. Steenbergen, N. Gaston, Chem. Eur. J. 21 (2015) 2862-2869.

[16] T.K. Ghosh, K. Tanaka, Y. Mochizuki, J. Mol. Struct. (THEOCHEM) 451 (1998) 61-71.

[17] X. Tan, P.J. Dagdigian, J. Phys. Chem. A 107 (2003) 2642-2649.

[18] R. Tonner, N. Gaston, Phys. Chem. Chem. Phys. 16 (2014) 24244-24249.

[19] D. J. Henry, J. Phys. Chem. C 116 (2012) 24814 – 24823.

[20] D. J. Henry, J. Phys. Chem. C 117 (2013) 26269 – 26279.

[21] D. J. Henry, P. Szarek, K. Hirai, K. Ichikawa, A. Tachibana, I. Yarovsky, J. Phys. Chem. C 115 (2011) 1714-1723.

[22] K. Ichikawa, H. Nozaki, N. Komazawa, A. Tachibana. AIP Advances 2 (2012) 042195-1 - 042195-16.

[23] A. Tachibana, R.G. Parr, Int. J. Quantum Chem. 41 (1992) 527-555.

[24] Gaussian 09, Revision C.01, Frisch, M. J.; Trucks, G. W.; Schlegel, H. B.; Scuseria, G. E.; Robb, M. A.; Cheeseman, J. R.; Scalmani, G.; Barone, V.; Mennucci, B.; Petersson, G. A.; et al. Gaussian, Inc., Wallingford CT, 2009.

[25] M. Senami, K. Ichikawa, A. Tachibana, QEDynamics, http://www.tachibana.kues.kyoto-u.ac.jp/qed/index.html

[26] B. Delley, J. Chem. Phys. 92 (1990) 508.

[27] B. Delley, J. Chem. Phys. 113 (2000) 7756.

[28] A. Tachibana, J. Mol. Model 11 (2005) 301-311.

[29] P. Ordon, A. Tachibana, J. Mol. Model 11 (2005) 312-316.

[30] P. Szarek, Y. Sueda, A. Tachibana, J. Chem. Phys. 129 (2008) 094102.

[31] P. Szarek, A. Tachibana, J. Mol. Model 13 (2007) 651-663.

[32] W. Humphrey, A. Dalke, K. Schulten, J. Mol. Graphics 14 (1996) 33.

[33] W.L. DeLano, PyMOL, DeLano Scientific LLC, San Carlos, CA, USA.

[34] K. Ichikawa, H. Nozaki, A. Tachibana, Mater Sci. Forum 783-786 (2014) 2207-2212.

[35] H. Nozaki, Y. Ikeda, K. Ichikawa, A. Tachibana, J. Compt. Chem. 36 (2015) 1240-1251.

[36] L. Guo, Comput. Materials Sci. 45 (2009) 951-958.

[37] J.-Y. Yi, Phys. Rev. B 61 (2000) 7277-7279.

[38] B. Song, P.-I. Cao, J. Chem. Phys. 123 (2005) 144312.

[39] A. Goldberg, I. Yarovsky, Phys. Rev. B 75 (2007) 195403.

[40] L.G. M. Pettersson, C.W. Bauschlicher, T. Halicioglu, J. Chem. Phys. 87 (1987) 2205-2213.

[41] S. H. Yang, D.A. Drabold, J.B. Adams, A. Sachdev, Phys. Rev. B 47 (1993) 1567-1576.

[42] Q. Sun, Q. Wang, J.Z. Yu, V. Kumar, Y. Kawazoe, Phys. Rev. B 63 (2001) 193408.

[43] A. Mañanes, F. Duque, F. Méndez, M.J. López, J.A. Alonso, J. Chem. Phys. 119 (2003) 5128-5141.

[44] P. Chandrachud, K. Joshi, D.G. Kanhere, Phys. Rev. B 76 (2007) 235423-1 - 235423-8.